# Observation and diagnostic application of Kr K-Shell emission in Magnetized Liner Inertial Fusion experiments at Z

J. T. Clapp,[1, a)] R. C. Mancini,[1] E. C. Harding,[2] M. A. Schaeuble,[2] and A. J. Harvey-Thompson[2]
[1)]*Department of Physics, University of Nevada, Reno, 1664 N Virginia St, Reno, Nevada 89557, USA*
[2)]*Sandia National Laboratories, 1515 Eubank Blvd SE, Albuquerque, New Mexico 87123, USA*

(Dated: 4 September 2022)

In a series of Magnetized Liner Inertial Fusion (MagLIF) experiments performed at the Z pulsed power accelerator of Sandia National Laboratories beryllium liners filled with deuterium gas pressures in the 4 – 8 atm range, and a tracer amount of krypton were imploded. At the collapse of the cylindrical implosion temperatures in the 1 – 3 keV range and atom number densities of $\sim 10^{23}\text{cm}^{-3}$ were expected. The plasma was magnetized with a 10 T axial magnetic field. Krypton was added to the fuel for diagnosing implosion plasma conditions. Krypton K-shell line emission was recorded with the CRITR time-integrated transmission crystal x-ray spectrometer. The observation shows n=2 to n=1 line emissions in B-, Be-, Li- and He-like Kr ions, and is characteristic of the highest electron temperatures achieved in the thermonuclear plasma. Detailed modeling of the krypton atomic kinetics and radiation physics permits us to interpret the composite spectral feature, and it demonstrates that the spectrum is temperature sensitive. We discuss temperatures extracted from the krypton data analysis for experiments performed with several filling pressures.

## I. INTRODUCTION

Magnetized Liner Inertial Fusion (MagLIF)[1] is an approach for controlled nuclear fusion that incorporates aspects from both Inertial Confinement Fusion (ICF) and Magnetic Confinement Fusion (MCF). Typical ICF concepts generally require high implosion velocities ($>$ 300 km/s) and spherical compression to create ignition[2]. MagLIF significantly relaxes these constraints while allowing for cylindrical compression by raising the initial temperature of deuterium fuel contained within a Beryllium metallic liner. This preheating coupled with the implementation of an external magnetic field allows for thermonuclear conditions to be achieved. It is characterized by three distinct phases: magnetization, pre-heating, and compression. The fuel is first magnetized with a 10 T external magnetic field to limit thermal conductivity in the radial direction. Then the Z-beamlet laser preheats the deuterium to roughly 500 eV to reduce the convergence ratio typical of cylindrical implosions from $\sim$ 120 to roughly 30. Lastly, a 20 MA current from the Z machine drives a $\vec{J} \times \vec{B}$ force to compress the liner on its axis, compressing deuterium gas contained within the liner to thermonuclear temperatures and densities.

Producing efficient nuclear fusion requires high peak temperatures. MagLIF has thus far achieved peak ion temperatures up to 3.1 keV at the end of the implosion[3]. Compared to other ICF and MCF approaches MagLIF is a relatively new concept, and the limited experiments conducted contain an abundance of information ripe for analysis. While the progress achieved so far has shown MagLIF as a promising candidate for controlled fusion, there are still many obstacles to overcome for positive energy production to be achieved. Accordingly, techniques to benchmark and accurately diagnose the conditions in an experiment are invaluable to the advancement of MagLIF.

Plasma spectroscopy has proven to be a valuable non-invasive tool for diagnosing plasma conditions achieved during high energy density experiments. Previously, success has been shown in diagnosing the preheating phase of MagLIF using Argon as a trace element[4,5]. However, the fuel is expected to reach temperatures $>$ 2 keV during the compression of the Be liner. Argon becomes highly ionized above 2 keV and thus loses its diagnostic capabilities at the latter stages of the implosion. Krypton, with an atomic number of 36, does not become fully ionized until $\approx$ 17 keV and therefore is an ideal candidate for spectroscopic analysis in the anticipated temperature range.

In six experiments at the Z machine, Krypton was added as a spectroscopic tracer. Analysis of the K-Shell line emission provides a method for diagnosing each experiment with an electron temperature throughout the duration of the implosion's collapse. By creating synthetic spectra through collisional-radiative modeling the Kr K-shell is seen to have sensitivity to electron temperature in the range of 2-4 keV. An analysis is done to determine a best fit between model and data to properly diagnose each shot with an electron temperature. The structure of the paper is as follows: section II discusses the general schematic of MagLIF as well as the experimental parameters of the six shots with a Kr tracer, section III introduces the spectral modeling used for Kr K-Shell line emission and the conditions we used to create the synthetic spectra, and section IV provides the results of the analysis and possible sources of improvement.

## II. EXPERIMENTAL DESIGN AND DATA

Each experiment presented here consisted of a cylindrical metallic Be liner 10 mm in height and 4.65 mm in diameter. The fuel was first magnetized with a 10 T magnetic field and

[a)]The author to whom correspondence may be addressed: jclapp@unr.edu

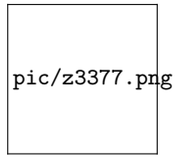


FIG. 1: Kr n: 2-1 emission collected from CRITR for shot z3377. Three distinct peaks can be identified. The peak on the right corresponds to the the He-$\alpha$ resonance line.


FIG. 2: The charge state distribution seen from a range of temperatures in the PrismSPECT simulation. The lower temperature bound has an average charge state of Be-like ions. As the temperature increases the charge state moves towards He-like ions. H-like charge state does not appear as the temperature required to significantly ionize the closed $1s^2$ shell exceeds temperatures present in these calculations.

then pre-heated with the 527 nm Z-beamlet laser[6] to approximately 500 eV[4,5]. The cylinder collapses on axis driven by a $\sim 17$ MA axial current produced by the Z pulse power driver[7] creating a massive rise in temperature and density. The details of each shot are shown in table I.

During the implosion and stagnation the Kr tracer ionizes and emits x-ray radiation that is collected by the axially resolving, compact, rugged in-chamber transmission (CRITR-AR) spectrometer[8]. This instrument is a Cauchois type spectrometer which fields a cylindrically-bent quartz crystal which axially resolves radiation in the range of 7-28 keV. The light is recorded with a FUJI TR image plate with an intrinsic resolution of $\approx 60\ \mu m$. Utilizing an imaging slit provides 1 mm resolution at the object plane. From this, time-integrated measurements of Kr K-shell emission at a photon energy of 13 keV are collected. The spectrometer has a resolving power of approximately $\lambda/\delta\lambda \approx 500$ in the region of interest. The resolution afforded by CRITR is modest but still captures significant emission from the Kr tracer.

Throughout the six experiments, the initial fill density and concentration of Kr was varied up to 100%. It should be noted that shots z3371 and z3377 had a wall thickness of 0.318 mm as opposed to the thickness of 0.465 mm of the other four. Previous LASNEX simulations of integrated MagLIF experiments have shown that the presence of Kr greatly affects the neutron yield if the atomic fraction of the tracer exceeds $\approx 0.001\%$[9]. Therefore, the Kr must be in small enough concentrations as to not affect the dynamics of the experiment.

An example of the emission collected by CRITR is shown in figure 1. For the purpose of the analysis presented here the spectra has been spatially integrated and the axial resolution will be the focus of future investigations. As the temperature increases during the implosion the Kr tracer will emit K-shell radiation at all points along the rise to peak temperatures. CRITR is a time-integrated instrument so the resulting spectra is not indicative of just one temperature and is a composite of all temperatures from the beginning to the end of the implosion's collapse.

## III. ATOMIC MODELING

The observed spectra shows Kr exhibiting an envelope of K-shell emission around 13 keV. Previous investigations have shown higher Z elements to exhibit a similar K-shell structure sensitive to various plasma properties[10]. To investigate the sensitivity of the Kr K-shell emission to electron temperature, the collisional-radiative spectral analysis code PrismSPECT was used[11]. To properly create synthetic spectra, the program must be supplied with an energy level structure and corresponding atomic cross-sections and rate coefficients. An atomic model was created using the Atomic Model Builder program from PRISM Computational Sciences. A total of over 8000 levels were included in the model. Since the emission observed is mostly composed of highly ionized charged states, Ne-like through fully stripped Kr energy levels were included in the model.

To create synthetic spectra, PrismSPECT uses a collection of atomic processes to calculate the emergent spectra from a given a set of initial conditions. The fill conditions were chosen according to the Kr concentration for each experiment as shown in table I with the remaining contents attributed to deuterium. We use a non-local thermodynamic equilibrium (NLTE) calculation with a slab geometry. A NLTE calculation is necessary because radiative effects in the plasma are non-negligible and collisions do not solely contribute to the level populations. Since a cylindrical geometry is not included as an option in PrismSPECT a slab geometry was chosen as to closely resemble the experimental design. Previous publications report radii at the end of MagLIF implosions to be $\sim 75\ \mu$m[12]. The thickness of the slab is then taken to be the average chord length through a circle with a radius of 75 $\mu$m. The mass densities are found through a mass conservation calculation, using the initial fill densities and volumes while assuming the final volumes of the cylinder. The electron temperature is then included as an independent variable. We calculated synthetic spectra for the conditions previously described for thirty different electron temperatures between 1500-2950 eV separated by 50 eV.

PrismSPECT outputs a charge state distribution and spectrum for a selected electron temperature. A charge state distribution for a few temperatures of interest is shown in figure 2. Even at temperatures as low as 1500 eV there is very little C-like emission and the entirety of the spectrum is mostly dominated by B-like through He-like charge states with the average charge state shifting higher with increasing temperature. The ionization potential of He-like Kr is 17.3 keV, so it is not expected for any H-like emission to appear in the spectra.

The bound-bound Kr K-shell transitions with corresponding ion emission contributions at 2500 eV are shown in figure 3. The calculated optical depth of the He-$\alpha$ resonance line is much less than one, implying the effect of radiation transport

TABLE I: Experimental design of six MagLIF shots

| Shot | Fill Density | Concentration | B-Field | Liner Diameter (wall thickness) |
|---|---|---|---|---|
| z3079 | 0.7 mg/cc | 0.00055% | 10 T | 4.65 mm (0.465 mm) |
| z3123 | 0.7 mg/cc | 0.00055% | 10 T | 4.65 mm (0.465 mm) |
| z3143 | 1.05 mg/cc | 0.0003% | 10 T | 4.65 mm (0.465 mm) |
| z3210 | 0.7 mg/cc | 0.00055% | 10 T | 4.65 mm (0.465 mm) |
| z3371 | 1.4 mg/cc | 0.0003% | 10 T | 4.65 mm (0.318 mm) |
| z3377 | 1.4 mg/cc | 0.0003% | 10 T | 4.65 mm (0.318 mm) |

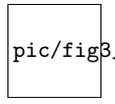


FIG. 3: Bound-bound Kr emission spectra produced for $T_e = 3000\ eV$. The entirety of the emission is produced by He through B-like transitions. There is no significant H-like emmision observed.


FIG. 4: Synthetic spectra created through the PrismSPECT calculation for varying electron temperatures adjusted for the expected resolving power of CRITR ($\approx 500$). Each spectra have been normalized to the prominent Li-like spectral feature at 13053 eV.

is negligible for the low concentrations of Kr in these experiments.

An overlay of each temperature included in the calculation is shown in figure 4. All spectral lines are normalized to the prominent Li-like spectral feature around 13053 eV. One can see that as the temperature increases, the intensity of the Li-, Be-, and B-like satellites decreases at a larger degree than the He-like emission increases. For this reason, the analysis has more sensitivity at lower temperatures. Also there is no significant H-like emission in this temperature range, and we do not anticipate recovering any in the experiments. Likewise, the He-$\beta$ spectral feature at 15.4 keV is too weak for these temperatures and is not included in the analysis. These spectra show a high degree of temperature sensitivity, allowing for use as a diagnostic in these experiments.

## IV. RESULTS

The data and the synthetic spectra are compared to find a best fit. For the purposes of this study, the underlying continuum is subtracted from each shot by fitting the left and right of the emission envelope to a line and subtracting the signal to produce only bound bound Kr emission. We use a weighted $\chi^2$ minimization analysis to match each experimental spectrum to a model spectrum. We use a $\chi^2$ of the form

$$\chi^2 = \frac{1}{N-1}\sum_{i=1}^{N}\left(\frac{I_{ei}(\nu) - aI_{ti}(\nu)}{\sigma_i}\right)^2 \quad (1)$$

where N is the total number of points sampled in the data, $I_{ei}$ is each experimental data point in the K-shell emission, $a$ is a scaling constant to adjust the units of the model intensity to that of the data, $I_{ti}$ is the corresponding point in the model and $\sigma_i$ is the standard deviation. The synthetic spectra produced in PrismSPECT calculate the emergent intensity in units of $erg/(cm^2 \times ster \times s \times eV)$, while the data is collected in terms of exposure on a TR image plate after reflecting off of a mirror and passing through different filters. Therefore it is necessary to scale the intensity of the model by the constant $a$. Since the entire spectrum is scaled by a single number, the minimum $\chi^2$ has an analytic solution for the value of $a$ and is found algebraically. The standard deviation is assumed not to vary with increasing photon energy of a given shot and is estimated from continuum statistics on either side of the emission envelope and fitting the resulting histogram to a Gaussian.

A summary of the results are shown in table II. The data is plotted along with the synthetic spectra that produced the minimum $\chi^2$ in figure 5. These temperatures are reasonable and comparable with previous published values of peak temperatures under the current design of MagLIF. From the raw data received, shot z3377 had the brightest Kr signal as well as the largest neutron yield and we obtained the highest value of temperature of the six shots from this analysis. Additionally, shot z3079 produced the least number of neutrons and also produced the lowest electron temperature. Shot z3143 has been published in a different study with an ion temperature of 2.1±20% keV, which is consistent with the results presented here[9].

The analysis is more sensitive at lower temperatures and becomes less sensitive as the temperature increases. As seen in figure 4, as the temperature rises, the Li, Be, and B-like emission lose intensity relative to the prominent Li-like spectral feature near 13053 eV at a larger rate than the He-$\alpha$ resonance strengthens. Therefore the $\chi^2$ analysis is asymmetric from lower to higher temperatures.

The "goodness" of the fits is determined if the minimum $\chi^2$ is of order 1. While the minimum $\chi^2$ values are reasonable, we see that each fit is not of order 1, suggesting that our fits could be better. There are a few reasons for this. For

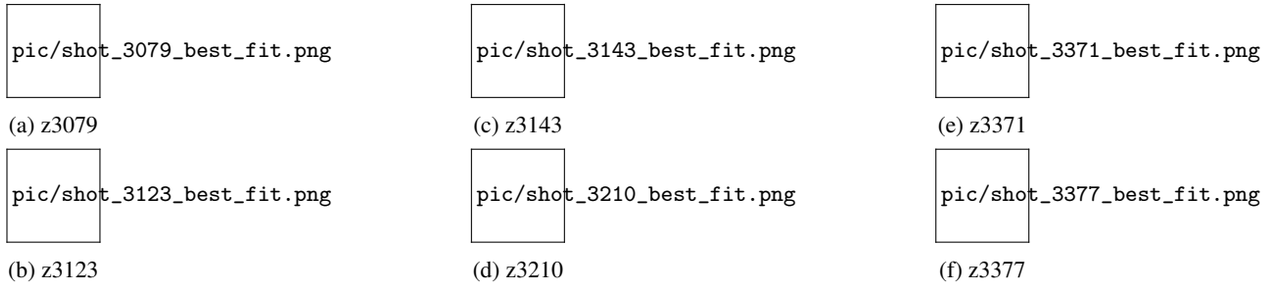


(a) z3079 (c) z3143 (e) z3371

(b) z3123 (d) z3210 (f) z3377

FIG. 5: The experimental data overlaid with the best fit temperature found through a $\chi^2$ minimization. Shots shown: a) z3079, b) z3123, c) z3143, d) z3210, e) z3371 and f) z3377

TABLE II: Results of the analysis

| Shot | $T_e$ (eV) | Reduced $\chi^2$ |
|---|---|---|
| z3079 | $2100^{+56}_{-12}$ | 6 |
| z3123 | $2350^{+3}_{-25}$ | 18 |
| z3143 | $2300^{+15}_{-25}$ | 12 |
| z3210 | $2350^{+54}_{-37}$ | 4 |
| z3371 | $2250^{+17}_{-11}$ | 27 |
| z3377 | $2450^{+3}_{-7}$ | 40 |

one, CRITR collects time-integrated spectra, and the Kr spectral data received is all of the emission from the beginning of the implosion until the stagnation which includes the emission from all temperatures between the initial and final stages of the implosion. Therefore attempting to model the emission with one temperature may be overly simplistic. Additionally, the synthetic spectra are created with an assumed final density based on previous publications. More investigation needs to be done to understand the density sensitivity of the Kr K-shell emission. These factors could contribute to better fits in the future.

## V. CONCLUSIONS

We have presented the first diagnostic application of a Kr tracer in MagLIF experiments at Z. The temperature reached during the cylindrical implosion ionizes Kr through He-like charge states. The collisional-radiative properties of the resulting plasma produce $n = 2 \rightarrow 1$ transitions which are sensitive to electron temperature. By modeling this emission and comparing the emergent spectra with the data, we have diagnosed each of the six shots with an electron temperature.

While this analysis has shown potential, there is significant progress to be done to provide better fits. As shown in table II the $\chi^2$ values are not of order 1. We plan to implement a more comprehensive multi-temperature analysis to provide better fits for the experimental data. We also plan on analyzing the Kr K-shell sensitivity to electron density to see if this has an effect on the emergent spectra.

Additionally, there appear to be significant differences between theory and experiment. The data shows a dip between the Li-like emission and the He-$\alpha$ resonance line whereas the simulation shows a slight bump at the He-$\alpha$ before falling off. This could result because the model calculates a Li-like satellite at a higher photon energy than is seen in the experiment, causing the prominent Li-like feature and the He-$\alpha$ to blend. Additionally, the model shows significant emission from B-like satellites that do not appear in the data. These issues will be investigated and discussed in a later publication.

## VI. ACKNOWLEDGMENTS

We would like to acknowledge Enac Gallardo-Diaz for his useful discussions concerning Kr K-Shell emission and spectral modeling. We would also like to thank Kyle Swanson, Jeffrey Rowland, Haritha Hariharan, Georges Jaar, and Aidan Klemmer for their valuable insights to the analysis presented here.

This work is supported by a contract from Sandia National Laboratories. Sandia National Laboratories is a multimission laboratory managed and operated by National Technology & Engineering Solutions of Sandia, LLC, a wholly owned subsidiary of Honeywell International Inc., for the U.S. Department of Energy's National Nuclear Security Administration under contract DE-NA0003525. This paper describes objective technical results and analysis. Any subjective views or opinions that might be expressed in the paper do not necessarily represent the views of the U.S. Department of Energy or the United States Government.

[1] S. A. Slutz, M. C. Herrmann, R. A. Vesey, A. B. Sefkow, D. B. Sinars, D. C. Rovang, K. J. Peterson, and M. E. Cuneo, Physics of Plasmas **17**, 056303 (2010).

[2] J. Lindl, P. Amendt, R. Berger, S. Glendinning, S. Glenzer, S. Haan, R. Kauffman, O. Landen, and L. Suter, Physics of Plasmas **11**, 339 (2004).

[3] M. Gomez, S. Slutz, C. Jennings, D. Ampleford, M. Weis, C. Myers, D. Yager-Elorriaga, K. Hahn, S. Hansen, E. Harding, A. Harvey-Thompson, D. Lamppa, M. Mangan, P. Knapp, T. Awe, G. Chandler, G. Cooper, J. Fein, M. Geissel, M. Glinsky, W. Lewis, C. Ruiz, D. Ruiz, M. Savage, P. Schmit, I. Smith, J. Styron, J. Porter, B. Jones, T. Mattsson, K. Peterson, G. Rochau, and D. Sinars, Physical Review Letters **125**, 155002 (2020).

[4] K. Carpenter, R. Mancini, E. Harding, A. Harvey-Thompson, M. Geissel,

M. Weis, S. Hansen, K. Peterson, and G. Rochau, Physics of Plasmas **27**, 052704 (2020).
[5]K. Carpenter, R. Mancini, E. Harding, A. Harvey-Thompson, M. Geissel, M. Weis, S. Hansen, K. Peterson, and G. Rochau, Physical Review E **102**, 023209 (2020).
[6]P. Rambo, I. Smith, J. Porter, M. Hurst, C. Speas, R. Adams, A. Garcia, E. Dawson, B. Thurston, C. Wakefield, J. Kellogg, M. Slattery, H. Ives, R. Broyles, J. Caird, A. Erlandson, J. Murray, W. Behrendt, N. Neilson, and J. Narduzzi, Applied Optics **44**, 2421 (2005).
[7]D. Rose, D. Welch, E. Madrid, C. Miller, R. Clark, W. Stygar, M. Savage, G. Rochau, J. Bailey, T. Nash, M. Sceiford, K. Struve, P. Corcoran, and B. Whitney, Physics Review ST Accel. Beams **13**, 010402 (2010).
[8]D. B. Sinars, D. F. Wegner, S. A. Pikuz, B. Jones, M. Geissel, S. B. Hansen, C. A. Coverdale, D. J. Ampleford, M. E. Cuneo, L. A. McPherson, and G. A. Rochau, Review of Scientific Instruments **82**, 063113 (2011).
[9]A. Harvey-Thompson, M. Weis, E. Harding, M. Geissel, D. Ampleford, G. Chandler, J. Fein, M. Glinsky, M. Gomez, K. Hahn, S. Hansen, C. Jennings, P. Knapp, R. Paguio, L. Perea, K. Peterson, J. Porter, P. Rambo, G. Robertson, G. Rochau, D. Ruiz, J. Schwartz, J. Shores, D. Sinars, S. Slutz, G. Smith, I. Smith, C. Speas, and K. Whittemore, Physics of Plasmas **25**, 112705 (2018).
[10]S. Regan, R. Epstein, B. Hammel, L. Suter, J. Ralph, H. Scott, M. Barrios, D. Bradley, D. Callahan, C. Cerjan, G. Collins, S. Dixit, T. Doeppner, M. Edwards, D. Farley, S. Glenn, S. Glenzer, I. Golovkin, S. Haan, A. Hamza, D. Hicks, N. Izumi, J. Kilkenny, J. Kline, G. Kyrala, O. Landen, T. Ma, J. MacFarlane, R. Mancini, R. McCrory, N. Meezan, D. Meyerhofer, A. Nikroo, K. Peterson, T. Sangster, P. Springer, and R. Town, Physics of Plasmas **19**, 056307 (2012).
[11]J. MacFarlane, I. Golovkin, P. Wang, P. Woodruff, and N. Pereyra, High Energy Density Physics **3**, 181 (2007).
[12]M. Gomez, S. Slutz, A. Sefkow, D. Sinars, K. Hahn, S. Hansen, E. Harding, P. Knapp, P. Schmit, C. Jennings, T. Awe, M. Geissel, D. Rovang, G. Chandler, G. Cooper, M. Cuneo, A. Harvey-Thompson, M. Hermann, M. Hess, O. Johns, D. Lamppa, M. Martin, R. McBride, K. Peterson, J. Porter, G. Robertson, G. Rochau, C. Ruiz, M. Savage, I. Smith, W. Stygar, and R. Vesey, Physical Review Letters **113**, 155003 (2014).

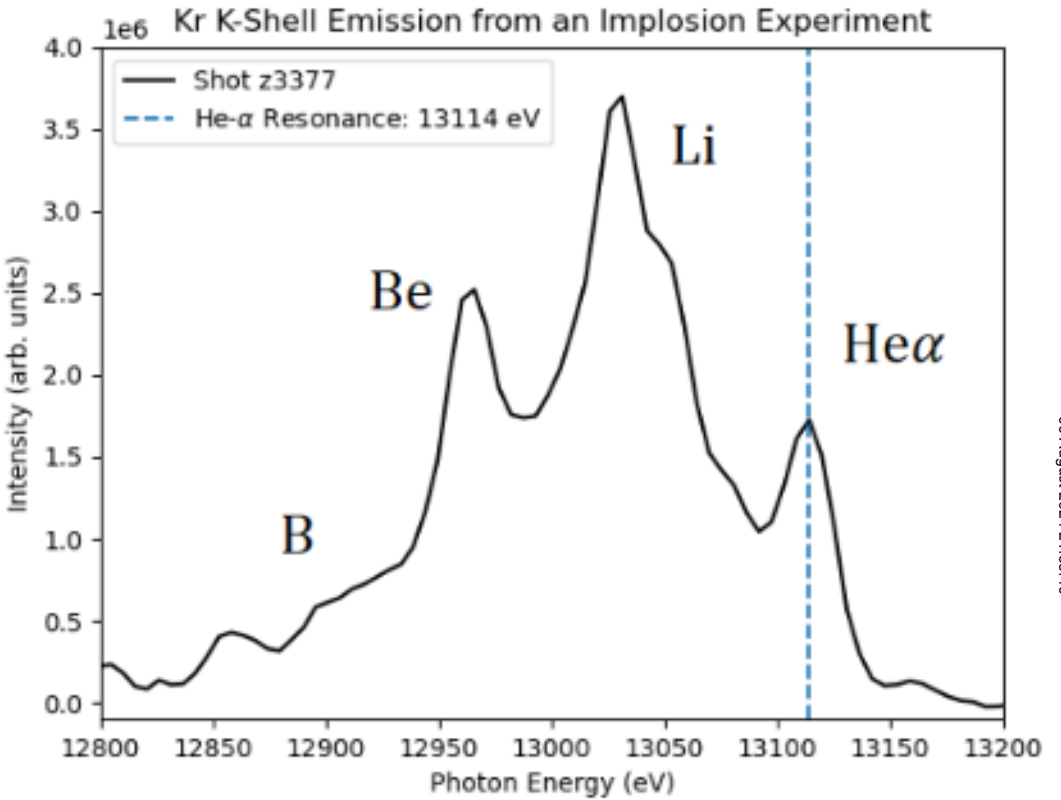


FIG. 1: Emission collected from CRITR for shot z3377. Three distinct peaks can be identified. The peak on the right corresponds to the the He-$\alpha$ resonance line.

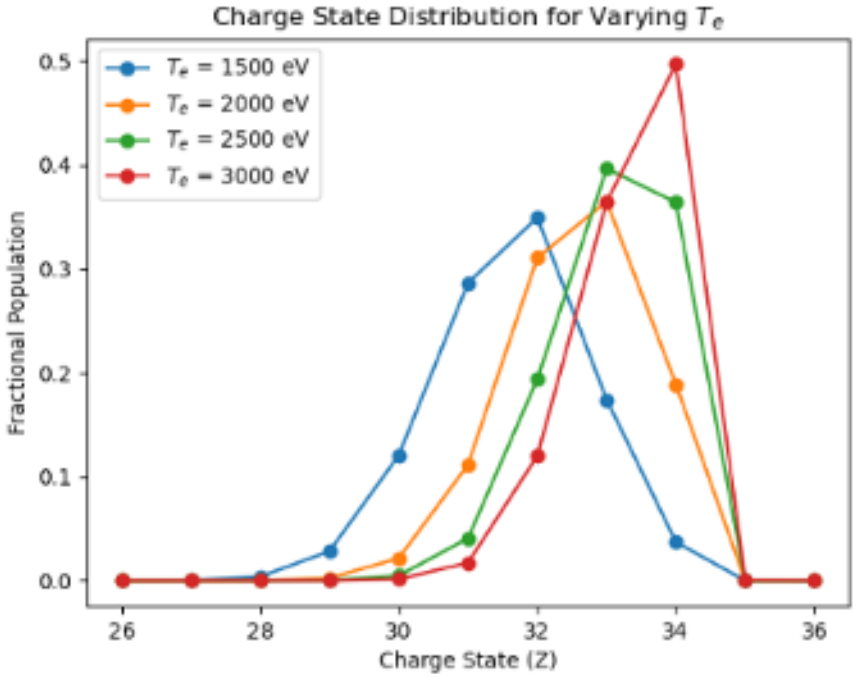


FIG. 2: The charge state distribution seen from a range of temperatures in the PrismSPECT simulation. The lower temperature bound has an average charge state of Be-like ions. As the temperature increases the charge state moves towards He-like ions. H-like charge state does not appear as the temperature required to significantly ionize the closed $1s^2$ shell exceeds temperatures present in these calculations.

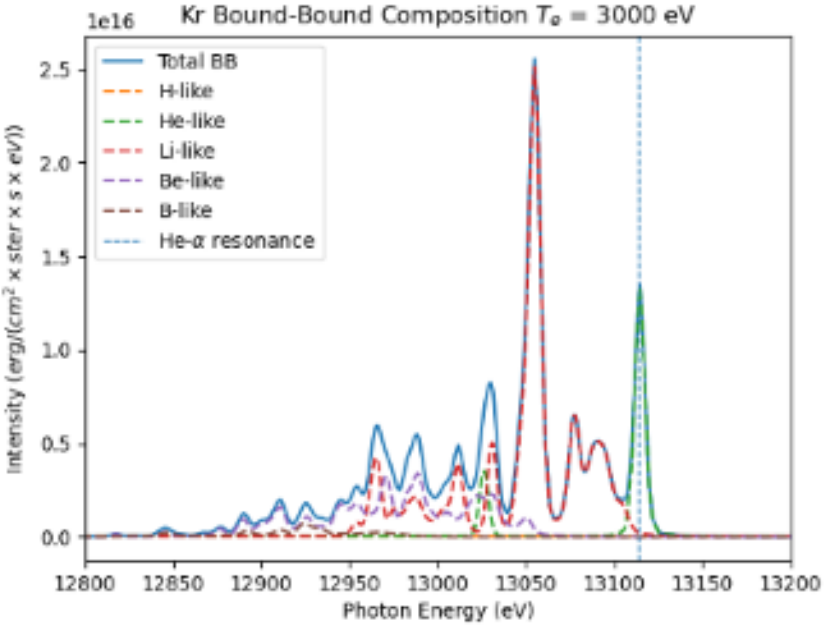


FIG. 3: Bound-bound Kr emission spectra produced for $T_e = 3000\ eV$. The entirety of the emission is produced by He through B-like transitions. There is no significant H-like emmision observed.

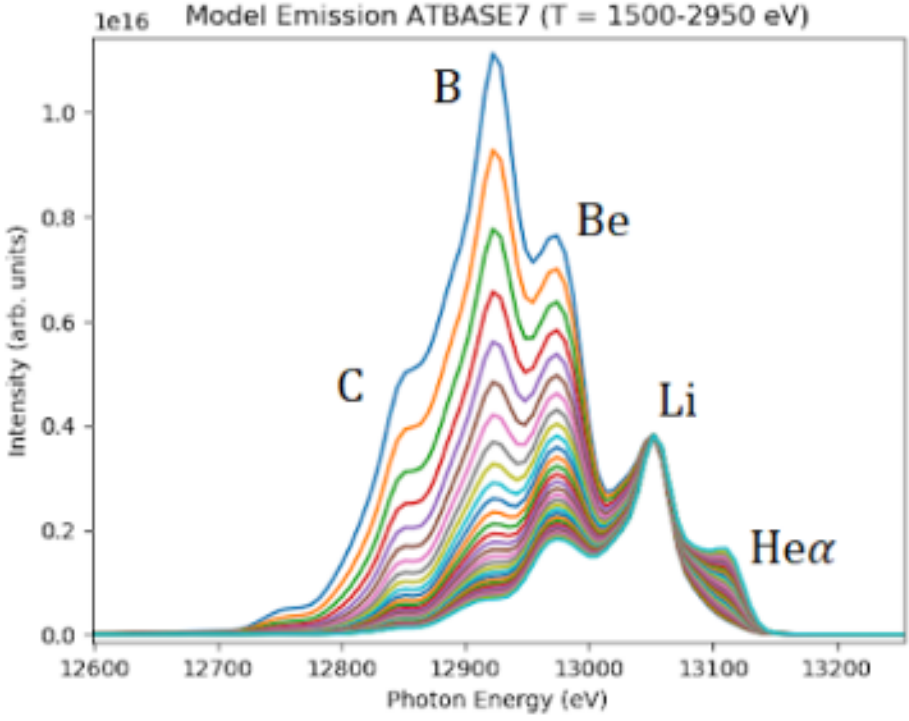


FIG. 4: Synthetic spectra created through the PrismSPECT calculation for varying electron temperatures adjusted for the expected resolving power of CRITR ($\approx 500$). Each spectra have been normalized to the prominent Li-like spectral feature at 13053 eV.

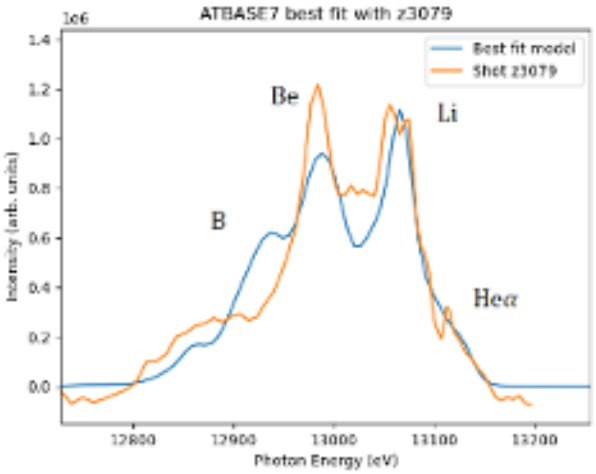


(a) z3079

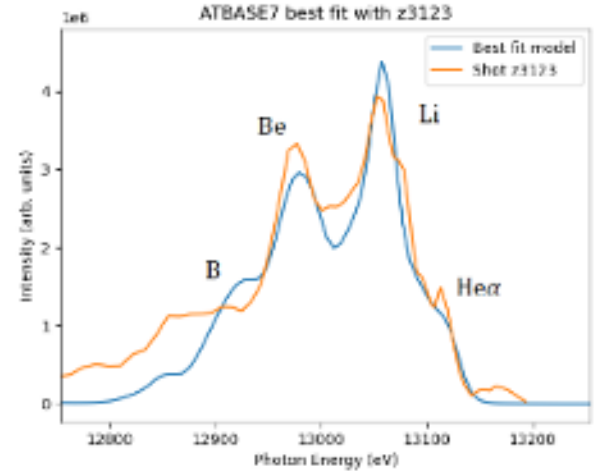


(b) z3123

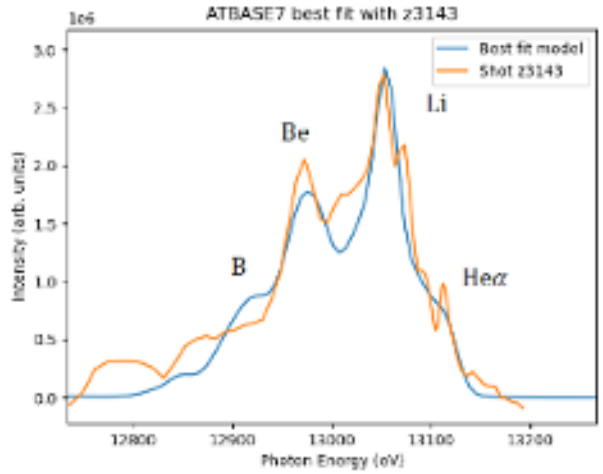


(c) z3143

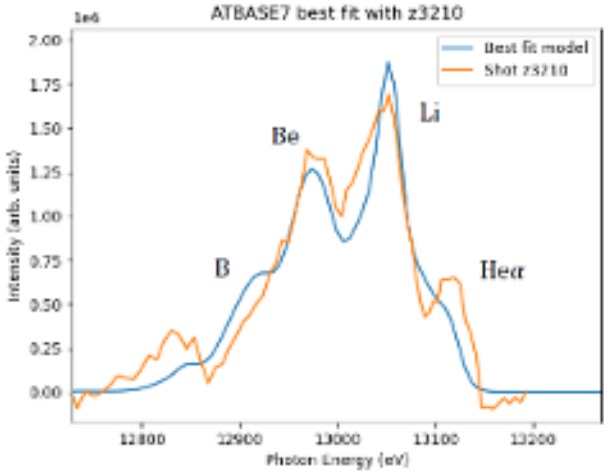


(d) z3210

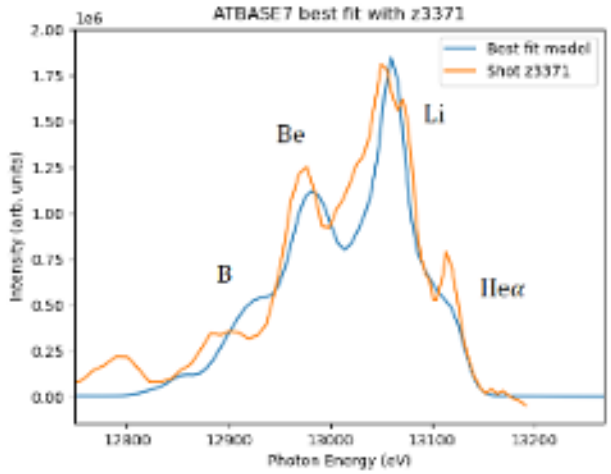


(e) z3371

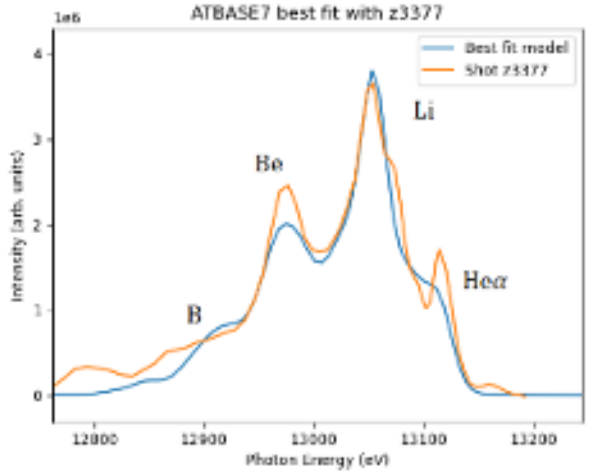


(f) z3377

FIG. 5: The experimental data overlaid with the best fit temperature found through a $\chi^2$ minimization. Shots shown: a) z3079, b) z3123, c) z3143, d) z3210, e) z3371 and f) z3377